International Journal of Bioprinting

RESEARCH ARTICLE

3D-printed PNAGA thermosensitive hydrogel-based microrobots: An effective cancer therapy by temperature-triggered drug release

Yan Zhou, Min Ye, Hongyu Zhao, Xiaopu Wang*

Shenzhen Institute of Artificial Intelligence and Robotics for Society (AIRS), The Chinese University of Hong Kong, Shenzhen, Guangdong 518129, China

Abstract

Hydrogels with temperature-responsive capabilities are increasingly utilized and researched owing to their prospective applications in the biomedical field. In this work, we developed thermosensitive poly-N-acryloyl glycinamide (PNAGA) hydrogels-based microrobots by using the advanced two-photon polymerization printing technology. N-acryloyl glycinamide (NAGA) concentration-dependent thermosensitive performance was presented and the underlying mechanism behind was discussed. Fast swelling behavior was achieved by PNAGA-100 at 45°C with a growth rate of 22.5%, which is the highest value among these PNAGA hydrogels. In addition, a drug release test of PNAGA-100-based thermosensitive hydrogels was conducted. Our microrobots demonstrate higher drug release amount at 45°C (close to body temperature) than at 25°C, indicating their great potential to be utilized in drug delivery in the human body. Furthermore, PNAGA-100-based thermosensitive microrobots are able to swim along the route as designed under the magnetic actuator after incubating with Fe@ZIF-8 crystals. Our biocompatible thermosensitive magnetic microrobots open up new options for biomedical applications and our work provides a robust pathway to the development of high-performance thermosensitive hydrogel-based microrobots.

Keywords: 3D printing; PNAGA thermosensitive hydrogel; Swelling; Drug release; Magnetic microrobot

***Corresponding author:**
Xiaopu Wang
(wangxiaopu@cuhk.edu.cn)

Citation: Zhou Y, Ye M, Zhao H, *et al*., 2023, 3D-printed PNAGA thermosensitive hydrogel-based microrobots: An effective cancer therapy by temperature-triggered drug release. *Int J Bioprint*, 9(3): 709.
https://doi.org/10.18063/ijb.709

Received: November 8, 2022
Accepted: December 22, 2022
Published Online: March 15, 2023

1. Introduction

Recent years have witnessed increasing interest in developing hydrogels because of their good mechanical properties, hydrophilicity, and biocompatibility[1-7]. Temperature-responsive hydrogels, which can autonomously change physical and/or chemical properties when temperature changes, are the research frontier of advanced functional materials science[8-11]. A series of temperature-responsive thermosensitive hydrogels have been reported in recent years[12-14]. Poly(n-isopropylacrylamide) (pNIPAM) is one of the prime examples with a low critical solution temperature (LCST) value close to human body temperature and exhibits obvious shrinkage properties around an LCST of ~32°C. pNIPAM has been widely used in many fields, such as drug delivery, tissue regeneration and artificial muscles[15-19].

In recent decades, scientists have devoted themselves to the development of thermosensitive hydrogels that exhibit swelling properties at temperatures close to the human body. Due to the lack of preparation technology and theoretical support[20-22], so far, only a few hydrogels with rapid swelling performance near body temperature have been successfully developed. Among them, Sun *et al.*[16] reported poly-N-acryloyl glycinamide (PNAGA)-type thermosensitive hydrogels, which produced obvious swelling effect at 45°C, and PNAGA composites have been widely used in tissue engineering[23,24], gripper[16,25], cancer therapy[26], etc.

However, the fabrication process of PNAGA is mainly based on the ultraviolet (UV) polymerization method[16,26-29]; therefore, it is not easy to obtain PNAGA-based 3D structures. This issue could be solved by introducing an advanced 3D printing technology called two-photon polymerization (2PP) as the fabrication method of PNAGA. 2PP, one of the most versatile and precise 3D printing techniques, uses models generated by computer-aided design (CAD) tools to fabricate 3D materials with sub-100 nm resolution[30], manifesting great advantages for fabricating PNAGA based hydrogels. First, 2PP utilizes femtosecond laser pulses of a near-infrared (NIR) laser beam to provide a nonlinear energy distribution at the center of the laser's focal point, resulting in the formation of aggregated 3D micro/nanostructures[31]. Second, 2PP does not require harsh processing environments (such as deep UV exposure or reactive ion etching) and harsh synthesis conditions (strong oxidants, toxic metal catalysts)[32]. Third, 2PP 3D technology can fabricate parts with complex geometries in a relatively short period of time, exhibiting the advantages of unprecedented precision, flexibility, high processing quality, and easy functionalization, and thus, this technology has been widely used in manufacturing research on the regeneration of biological microdevices and tissues such as bone, muscle, skin, and neurons, as well as organs such as trachea, liver, kidney, and heart[33-37].

Given the various advantages of 2PP 3D printing technology and the urgent need for enriching the synthetic approaches of PNAGA-based hydrogels to endow them with wider applications, we first report micro-sized PNAGA thermosensitive hydrogels prepared by 2PP 3D printing technology in this work. Our PNAGA hydrogels exhibit better swelling performance at 45°C than that at room temperature, at which PNAGA-100 microstructure manifests the best and fast swelling property with a growth rate of 22.5%. Particularly, PNAGA-100-based thermosensitive microstructures show higher drug release efficiency at 45°C (close to body temperature) than room temperature, indicating that they are promising candidates for drug release in the human body. After being decorated with zeolitic imidazolate framework-8 (Fe@ZIF-8), the thermosensitive PNAGA-based microstructures can achieve locomotion with the control of a magnetic field, acting as microrobots in water, which can be potentially applied in drug delivery and object transportation.

2. Materials and methods

2.1. Materials

N-acryloyl glycinamide (NAGA; purity: 98%) was purchased from Alfa (Zhengzhou, China), and water-soluble two-photon photo-initiator P2CK and Fe@ZIF-8 were prepared based on the protocols described in a research paper[38]. Crosslinker poly (ethylene glycol) diacrylate (PEGDA-575; 99.5%) was purchased from Sigma-Aldrich (Shanghai, China). N,N′-methylene bisacrylamide (MBAA, purity: 99%), ethanol and isopropanol (purity: 98%) were purchased from Energy Chemical (Anhui, China). All reagents were used directly without further purification. Deionized (DI) water from ultra-pure water machine was utilized throughout the experiments.

2.2. Instruments and measurements

The 2PP 3D printing of PNAGA was conducted by Nanoscribe GmbH. The micro-level Fourier-transform infrared spectroscopy (FTIR) spectrum of PNAGA-100 was obtained using spotlight 200i (PerkinElmer FTIR microscopy). The surface morphologies of these thermosensitive hydrogels were examined using Apreo2 S Lovac. Elastic modulus and energy storage modulus of PNAGA hydrogels were recorded by Discovery Series Hybrid Rheometer (DHR; TA Instruments, New Castle, USA). The swimming experiments of PNAGA-based magnetic microrobots were conducted using Magnebotix (MFG-100) and a self-built Helmholtz coil magnetic control system. The 3D-printed microstructures were examined by inverted fluorescence microscopy IX73P2F. The doxorubicin (DOX) release was determined by ELISA.

2.3. Thermosensitive measurement of 3D-printed PNAGA microstructures

PNAGA hydrogel-based microstructures were fabricated according to different recipes (Table 1) using 3D Direct Laser lithography (Nanoscribe GmbH). In detail, NAGA (50 mg; 100 mg; 200 mg; 300 mg), PEGDA-575 (200 μL) and P2CK (1 mg) were dissolved in 0.8 mL DI water, respectively. The mixture was stirred at room temperature for 10 min. Then, 15 μL mixture buffer was spin-coated on the glass substrate. The precursor solution was dipped in a round gasket on the glass and printed via 2PP (780 nm). Purified 3D structures were observed after developing in DI water three times for 5 min each time. The sizes of these PNAGA microstructures for thermosensitive measurement are 3D cubic structures with a side length of 100 μm and a

thickness of 5 μm. These microstructures were immersed in water at 25°C and 45°C, respectively.

$$\text{Growth rate (\%)} = (Vt - V0)/V0$$

where Vt refers to the volume of the cube after being immersed in water of 25°C or 45°C for t hours, and $V0$ refers to the initial volume of the cube after being immersed in water.

2.4. Drug release evaluation of 3D-printed PNAGA-100

PNAGA-100 thermosensitive microstructures were fabricated using a 3D Direct Laser lithography (Nanoscribe GmbH) according to the method described in section 2.3. Laser power used was 90 mW, and the scan speed was 3000 μm s^{-1}. We printed 1000 five-pointed stars with sides of 100 μm and a thickness of 5 μm. The five-pointed star structures were developed in DI water for 5 min and then dried with a nitrogen gun. Finally, these DOX-coated PNAGA-100 microstructures were immersed in water at 25°C and 45°C, respectively, to evaluate the drug release amount. The DOX release amount was determined by ELISA.

2.5. Biocompatibility measurement of 3D-printed PNAGA-based hydrogels

PNAGA-100 and PNAGA-300 were prepared according to the method mentioned above with the size of 100 × 100 × 5 μm. 3T3 cells in phosphate-buffered saline (PBS) buffer were incubated on the PNAGA-100 and 300 microstructures for 20 h in a carbon dioxide incubator.

2.6. Swimming demonstration of helix PNAGA-100-based microrobots under a magnetic field

The helix PNAGA-100 microrobots were prepared by 3D printing using Nanoscribe. The Nanoscribe was equipped with a femtolaser of 780 nm and the 25× objective was utilized in the experiment. First, PNAGA-100-based helix microrobots were synthesized with 140 μm body length and 50 μm screw diameter. Second, 20 mg Fe@ZIF-8 crystals were dispersed in 1 mL DI water and sonicated for 10 min. After that, these helix microrobots were incubated in Fe@ZIF-8 solution with a concentration of 20 mg/mL for 48 h. The swimming demonstration of magnetic microrobots was conducted using the equipment of Magnebotix (MFG-100). The manipulation pathway of the microrobots was tracked using ImageJ software.

3. Results and discussion

The key to the preparation of PNAGA micro/nanostructures using 2PP 3D printing technology is to find suitable initiators and coupling agents. According to the literature survey, we found that P2CK (sodium 3,39-((((1E,19E)-(2-oxocyclopentane-1,3-diylidene) bis (methanylylidene)) bis(4,1-phenylene))bis(methylazanediyl)) dipropanoate) is a water-soluble and efficient two-photon initiator[38], and we synthesized P2CK according to the method reported in the literature[39]. In addition, after experimental attempts, we successfully used PEGDA as a coupling agent to realize the 2PP 3D printing of PNAGA microstructures. In this section, the preparation method, temperature sensitivity test, drug release measurement, biocompatibility test, and magnetic control of the PNAGA microrobot are introduced in detail.

3.1. Synthetic scheme of PNAGA microstructures fabricated by 2PP 3D printing method

The 3D printing process of PNAGA hydrogels is illustrated in Figure 1. The mixture of monomer NAGA, two-photon initiator P2CK, crosslinker PEGDA and DI water was sonicated for 10 min to obtain a precursor solution. The precursor solution was dipped in a round gasket on the glass and printed via 2PP (780 nm). Purified 3D structures were observed after developing in DI water three times for 5 min each time. Solidwork software was utilized to design different 3D structures and prepare various PNAGA morphologies according to needs. According to the method described above, PNAGA hydrogel with different morphologies can be obtained. Figure 2a shows the chemical structure of 3D-printed PNAGA hydrogel, which consists of the thermosensitive unit PNAGA and the crosslinker PEGDA. Figure 2b presents an optical image of PNAGA hydrogel-based cubic microstructures.

3.2. 3D printing window of PNAGA-based microstructures

To assess the photocurability of the precursor solutions prepared using different recipes (Table 1), various scan speeds and laser powers were applied. PNAGA-50 can be successfully 3D-printed with a few parameters **Figure S1**). Figure 3a and b presents the 3D printing window and corresponding optical image of PNAGA-100. Cubic microstructures can be fabricated by varying laser powers and scan speeds. In detail, there are mainly three states (Figure 3c) formed with different printing parameters: (i) state with normal size (printed as designed); (ii) swelling state (larger than designed); and (iii) bending state. To the best of our knowledge, we assume that this is due to the variation of crosslinking density and the degree of energy absorbed by different layers in microstructures under different laser powers and scan speeds. In addition, PNAGA-200 and PNAGA-300 manifest three states similar to PNAGA-100. In contrast, the printing windows of PNAGA-200 and PNAGA-300 exhibited wider swelling and bending regions (**Figures S2 and S3**) compared to that of PNAGA-100. Possibly due

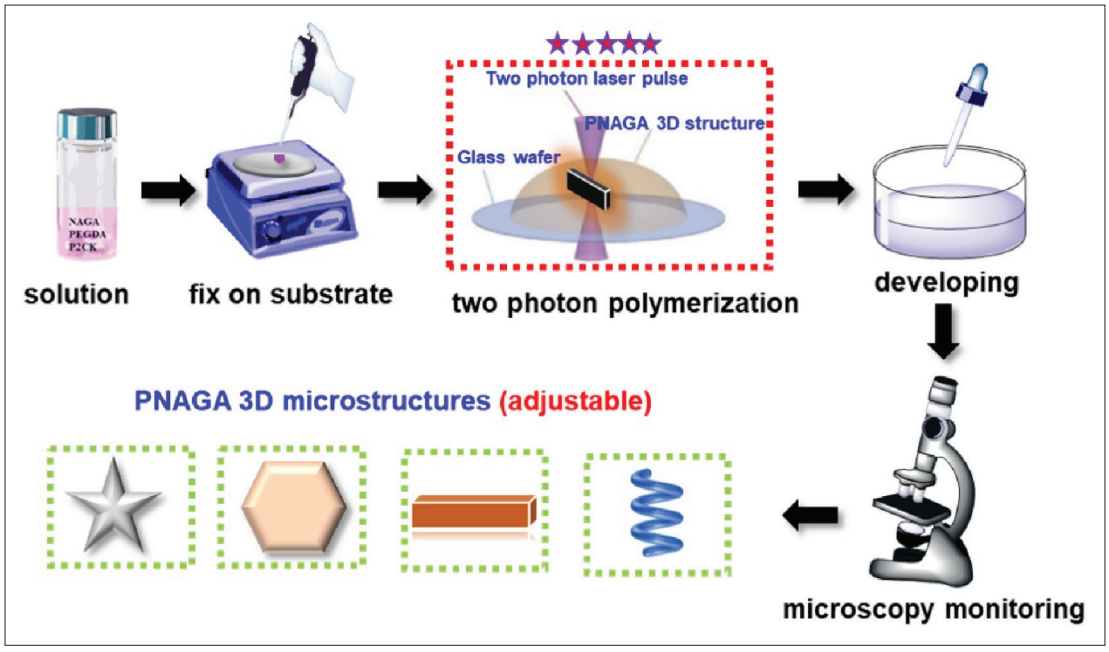

Figure 1. 3D printing (two-photon polymerization) process of PNAGA microstructures.

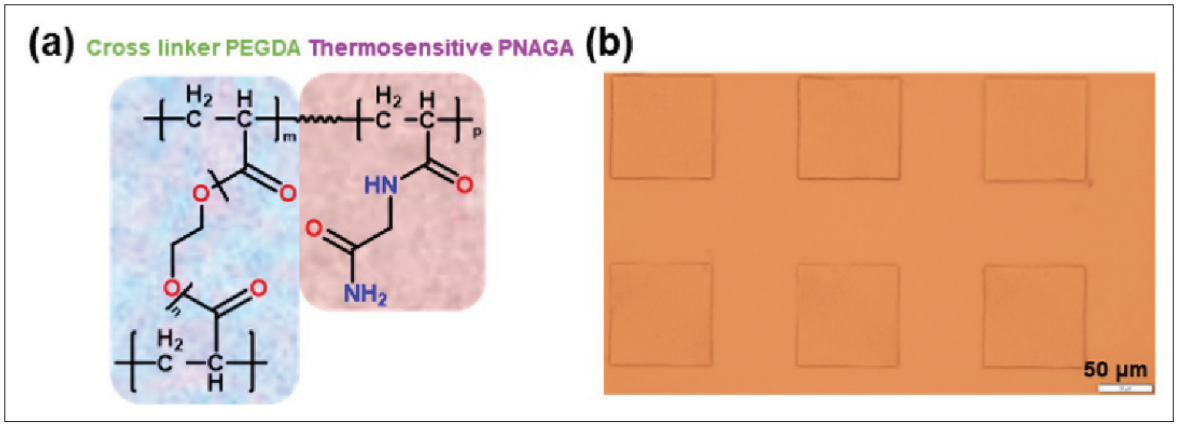

Figure 2. (a) Chemical structure of PNAGA-PEGDA. (b) Optical image of PNAGA hydrogel-based cubic microstructures.

Table 1. Recipes of PNAGA thermosensitive hydrogels

Sample name	Recipe
PNAGA-50	NAGA 50 mg; PEDGA 200 μL; P2CK 1 mg; H_2O 0.8 mL
PNAGA-100	NAGA 100 mg; PEDGA 200 μL; P2CK 1 mg; H_2O 0.8 mL
PNAGA-200	NAGA 200 mg; PEDGA 200 μL; P2CK 1 mg; H_2O 0.8 mL
PNAGA-300	NAGA 300 mg; PEDGA 200 μL; P2CK 1 mg; H_2O 0.8 mL

to the increase in polymer chain density with increasing NAGA monomer concentration, the degree of expansion for each layer is different and the interaction between branches is more complex, resulting in a diverse bending topography[40,41]. To our knowledge, the swelling and bending performance of hydrogels under light stimuli are mainly influenced by light conditions, shape/size, and mechanical properties of the hydrogels[42,43]. The variation of storage modulus G′ and loss modulus G″ for PNAGA-200 and PNAGA-300 (**Figure S4**), as compared to PNAGA-100, may lead to wider deformation 3D printing window.

3.3. Characterization

3.3.1. FTIR

To confirm the structure of PNAGA-100 synthesized by 3D printing technology via the 2PP method, the micro infrared spectroscopy of PNAGA-100 was conducted. As shown in Figure 4, the characteristic peak at 2923 cm^{-1} is attributed to the symmetric stretching vibrations of

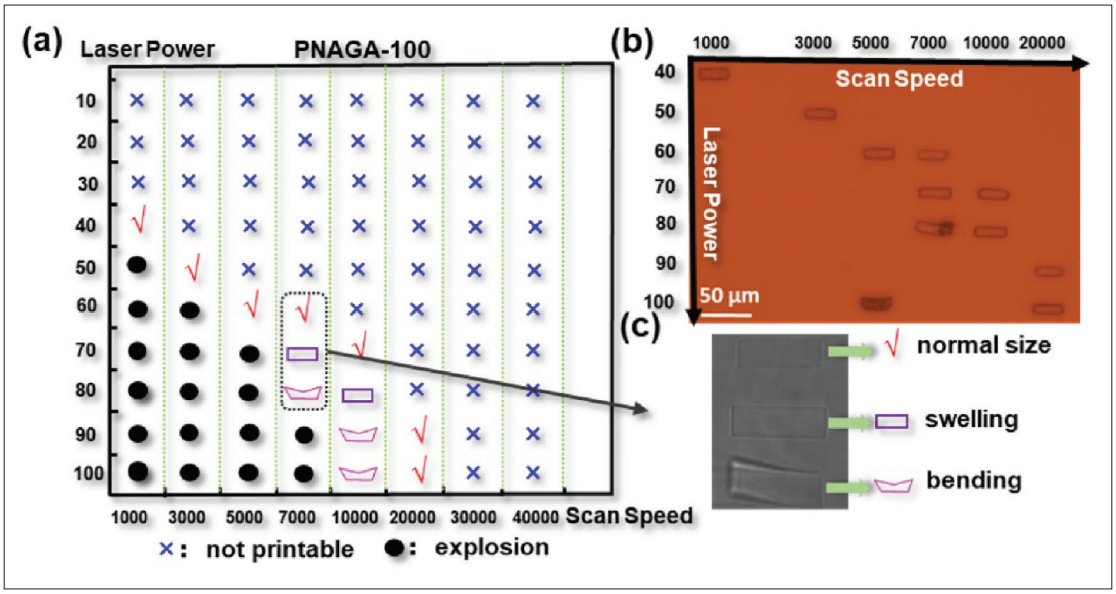

Figure 3. (a) 3D printing window of PNAGA-100 under different parameters. (b) Optical image of PNAGA-100 responding to the printing parameters in panel (a). (c) The three states of PNAGA-100 with different printing conditions.

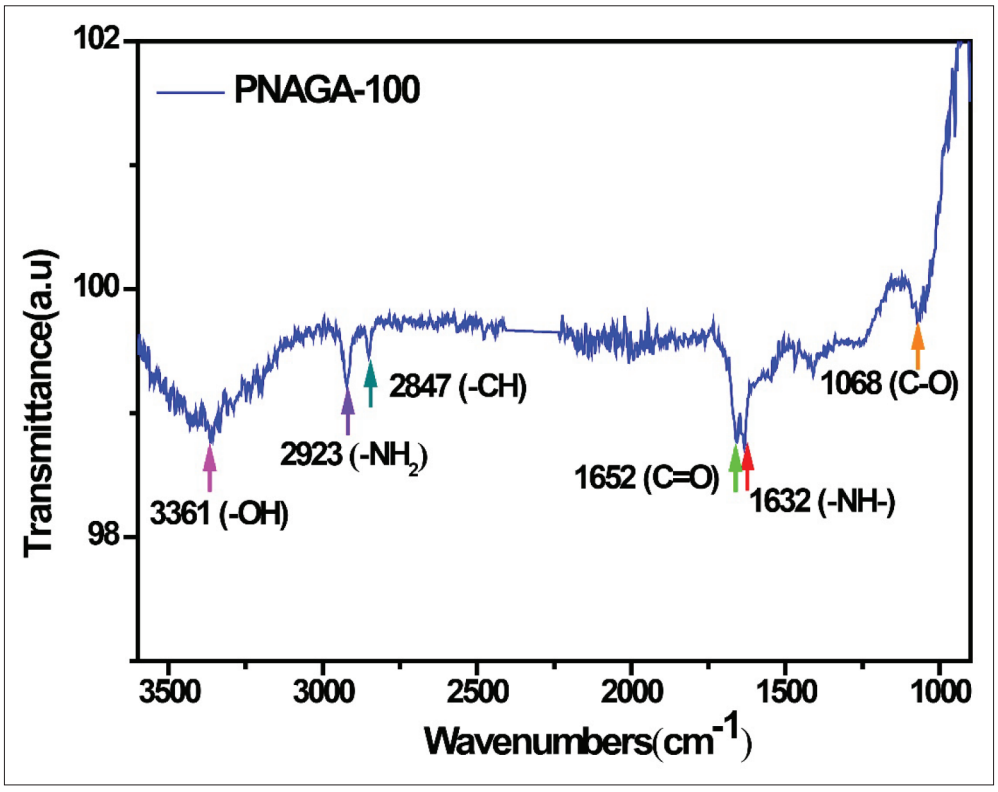

Figure 4. The FTIR spectra of PNAGA-100 synthesized by two-photon polymerization.

-NH- and the asymmetric stretching vibrations of -NH_2. The peak at 2847 cm^{-1} is assigned to vibrations of the -CH-. In addition, the strong peaks at about 1652 cm^{-1} and 1632 cm^{-1} are the vibrations of C=O and the bending vibration of -NH-, respectively. The C-O unit of PEGDA manifests vibrations peaks at 1068 cm^{-1}. There was an unobvious –OH vibration band at 3361 cm^{-1} rising from the terminal hydroxyl of PEGDA. It is hard to find the peak of C=C, proving the completion of the polymerization process.

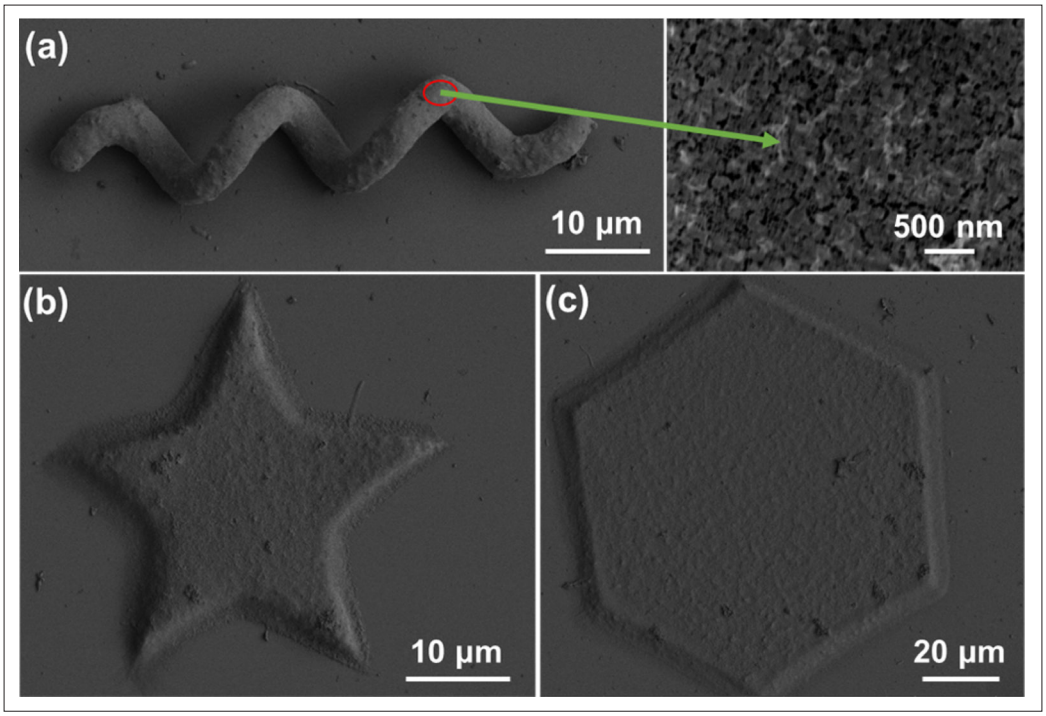

Figure 5. (a) SEM spectra of PNAGA-100 in helix shape. (b) SEM spectra of PNAGA-100 in five-pointed star pattern. (c) SEM spectra of PNAGA-100 hexagonal pattern.

3.3.2. Scanning electron microscopy

Figure 5 shows the scanning electron microscopy (SEM) images of PNAGA-100 microstructures prepared by 2PP method. Structure design with CAD software incorporated with advanced 3D printing technology makes it possible to obtain diverse shapes of PNAGA hydrogels with high resolution, high precision, and compact morphologies (Figure 5a). Helix, five-pointed star (Figure 5b), and hexagonal patterns (Figure 5c) of PNAGA-100-based microrobots were designed and successfully 3D-printed, and their sizes can be adjusted according to different application situations.

3.4. Thermosensitive properties of 3D-printed PNAGA microstructures

First, we prepared PNAGA microstructures with different NAGA loadings via the 2PP method to estimate the thermosensitive properties of materials (Table 1). As shown in Figure 6, the thermosensitive properties of these hydrogels were evaluated with different duration times (6 h; 12 h; 24 h) at room temperature (25°C) and 45°C, respectively. The growth rates of these hydrogels were measured for the sake of evaluating their swelling performance. In detail, the growth rates of these hydrogels were much higher at 45°C (close to body temperature) than that at 25°C, revealing that all these PNAGA-based microrobots exhibit better thermosensitive performance under 45°C. In addition, the growth rates of these microstructures were enhanced by increasing the monomer NAGA amount from 50 mg (PNAGA-50) to 100 mg (PNAGA-100). However, they decreased sharply when the NAGA amount was further increased to 200 mg (PNAGA-200) and 300 mg (PNAGA-300), indicating that NAGA concentration plays a vital role in modulating the thermosensitive performance of these materials. Noticeably, the optimized growth rate of PNAGA-100 was 22.5% when it was incubated in DI water at 45°C for 12 h. PNAGA-100 reached a growth rate of 20.8% in the shortest time (6 h), which demonstrates the best thermosensitive performance among these hydrogels. Furthermore, it is hard to evaluate the thermosensitive performance of PNAGA-300 after it was incubated in DI water at 45°C for 24 h owing to its preference for bending because of swelling (**Figure S5**).

Although we lack a comprehensive theory to explain why PNAGA-100 exhibits better thermosensitive performance than others, we rationalized this by the variations of PNAGA polymer structures induced by NAGA monomer concentrations. In detail, PNAGA has dual H-bonding donors (D) and dual H-bonding acceptors (A), which feature an ADAD hydrogen network (Figure 7). Based on the NAGA concentrations, the phase diagrams of PNAGA are mainly divided into two regions[44]. Region 1 has medium NAGA concentration, and swellable and thermosensitive hydrogels are observed with a gel-like behavior in this region. PNAGA-100 with higher NAGA

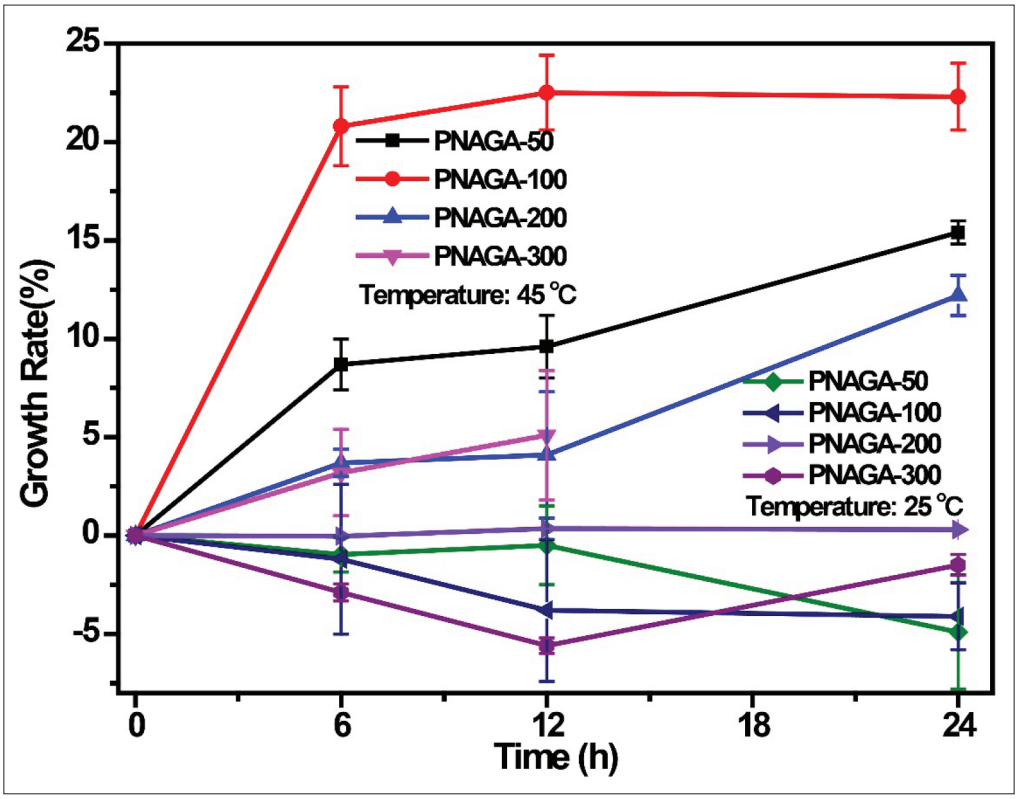

Figure 6. Thermosensitive properties of 3D-printed PNAGA-based microrobots under 25°C and 45°C.

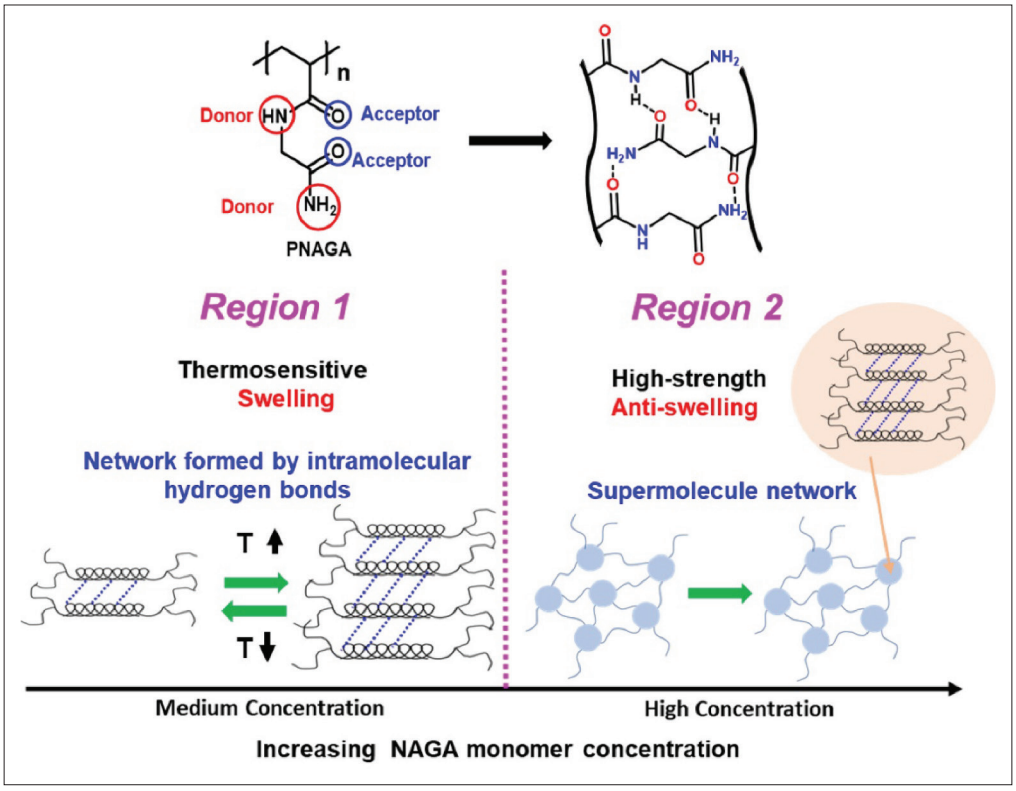

Figure 7. Different states of PNAGA with increased NAGA concentrations.

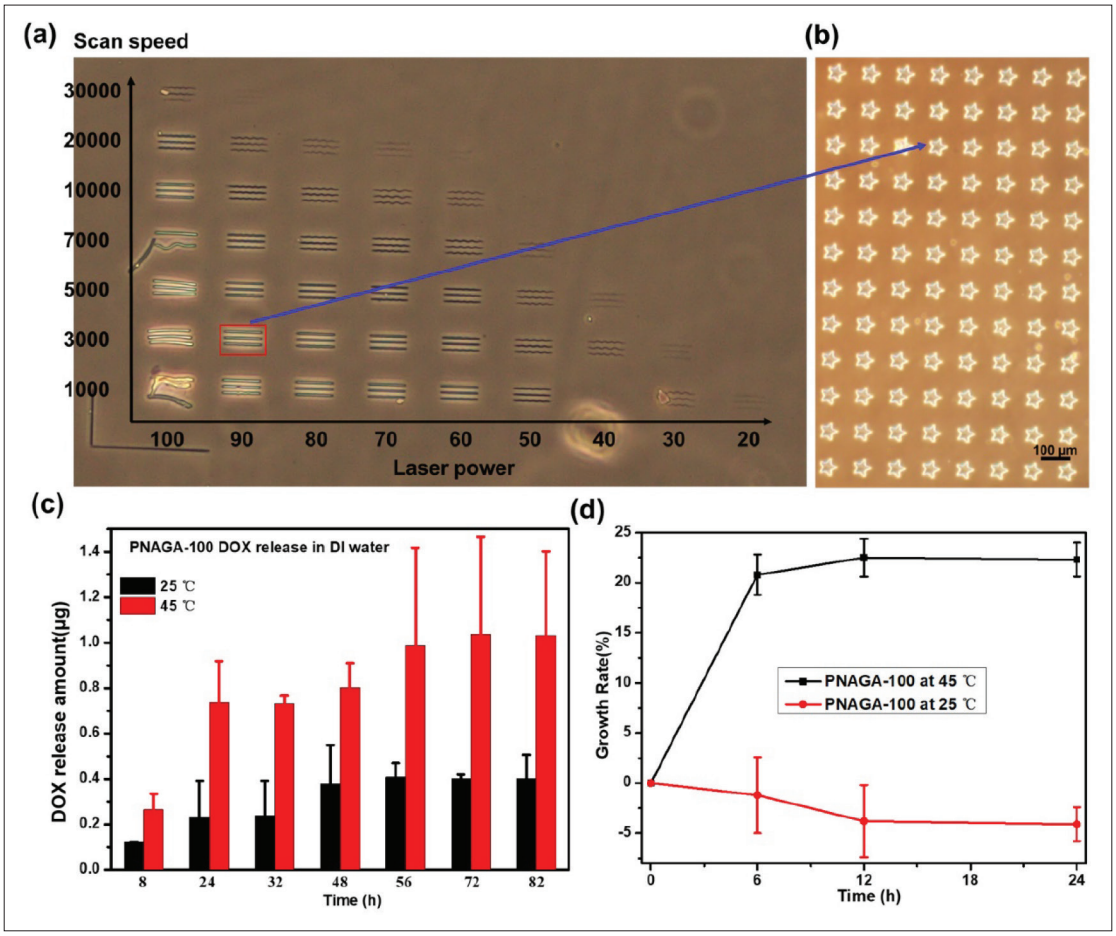

Figure 8. (a) 3D printing window of PNAGA-100-encapsuled DOX. (b) 3D structures of PNAGA-100-DOX printed via 2PP method. (c) DOX release measurement of PNAGA-100 under 25°C and 45°C, respectively. (d) Evaluation of thermosensitive properties of PNAGA-100.

concentration benefits the formation in a longer term and orderly hydrogen network when the temperature is increased, and thus exhibits better thermosensitive performance than PNAGA-50. However, in the region with a high concentration of NAGA (above 10 wt%) referred to as Region 2 in Figure 7, high-strength and robust supramolecular PNAGA hydrogels, which are equipped with nonthermosensitive and nonswellable features, were obtained[27]. As a result, PNAGA-100 with medium NAGA concentration manifests better thermosensitive performance than PNAGA-200 and PNAGA-300 with high-strength supramolecular networks. In terms of practical applications, different PNAGA systems can be selected based on the requirements by varying the NAGA concentrations.

3.5. Drug release

Taking into account the excellent thermosensitive performance of PNAGA-100, the drug release measurements were assessed with PNAGA-100 under 45°C and 25°C, respectively. Firstly, PNAGA-100 microstructures that encapsule DOX as drugs were 3D-printed via the 2PP method. Figure 8a shows the 3D printing window of PNAGA-100-DOX with varying laser powers and scan speeds. Taking laser power of 90 mW and scan speed of 3000 μm/s as an example, 3D structures of PNAGA-100-DOX in the shape of a five-pointed star with clear outlines were printed, proving that 3D printing of PNAGA-100-based thermosensitive microstructure with DOX via 2PP method can be successfully achieved with perfect 3D configuration (Figure 8b). Second, PNAGA-100-DOX based microstructures were incubated in DI water at 45°C and 25°C, respectively. The DOX release amount was evaluated by measuring the absorbance using a microplate reader. As displayed in Figure 8c, the DOX release amounts of PNAGA-100 at 45°C are about two to three times higher than that at 25°C under each incubation time, which agrees well with its thermosensitive performance (Figure 8d). At 45°C, higher DOX release amounts were observed, which may be due to the swelling state of PNAGA-100, benefiting the expansion of the porous structures on the surface of PNAGA-100-based hydrogels and thus contributing to

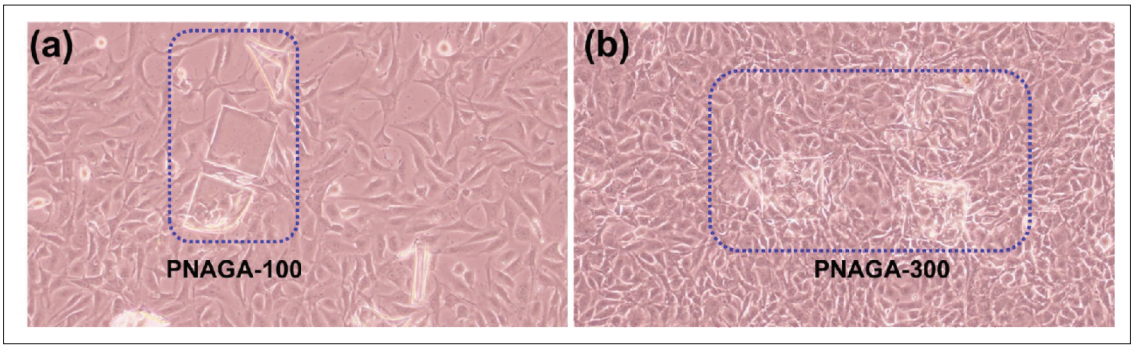

Figure 9. (a) PNAGA-100 and (b) PNAGA-300 incubated with 3T3 cells for 20 h.

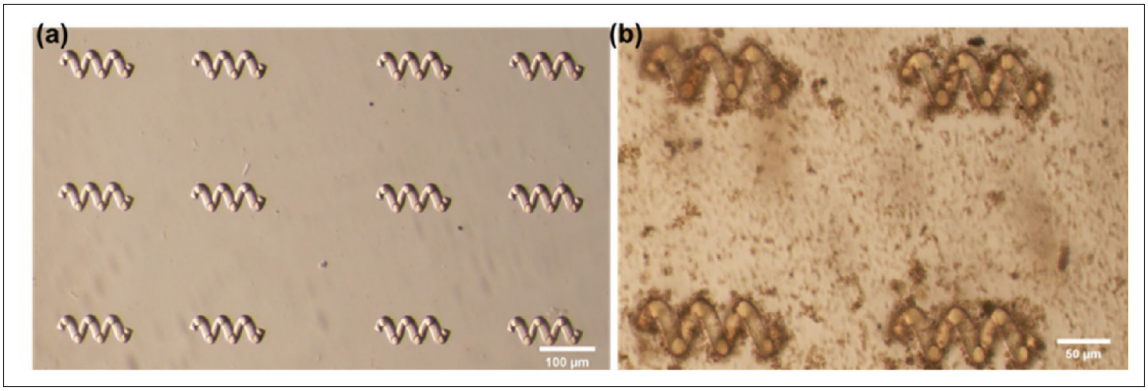

Figure 10. (a) Helix PNAGA-100-based thermosensitive microrobots fabricated by 3D printing. (b) Metal–organic framework (MOF)-coated magnetic helix PNAGA-100-based microrobots.

DOX release from PNAGA-100's network. In a word, PNAGA-100 with thermosensitive behavior induced by near-body temperature demonstrates great potential in drug release and cancer therapy *in vivo*.

3.6. Biocompatibility

To elucidate the biocompatibility of fabricated PNAGA hydrogel microstructures, we cultured 3T3 (human embryonic fibroblast) cells on PNAGA-100 and PNAGA-300 microstructures for 20 h. As shown in Figure 9, 3T3 cells grow well with PNAGA hydrogels, proving that the cytotoxicity of PNAGA microstructures is negligible.

PNAGA-100 hydrogel microstructures have good biocompatibility, high thermosensitive performance and hydrophilic properties, making them promising candidates to be utilized in various biomedical applications, such as drug release, tissue engineering and biosensors.

3.7. Motion control of thermosensitive PNAGA-100-based microrobots

The PNAGA-100 is designed with a spiral shape because it has been shown to be beneficial for the motion of small robots with low Reynolds numbers at small scales[45]. Helix PNAGA-100-based microrobots were synthesized via the 2PP method (Figure 10a). Taking advantage of the magnetic property, good biocompatibility, and biodegradability of Fe@ZIF-8[38], we loaded Fe@ZIF-8 crystals on the surface of PNAGA-100-based microrobots to ensure that the microrobots can be magnetically controlled. After 2 days of incubation, Fe@ZIF-8 crystals were coated on the microrobots surface in a uniform manner (Figure 10b).

Magnetically controlled locomotion of PNAGA-100-based helix microrobots were conducted within a rotating magnetic field of 15 mT and at 6 Hz. As shown in Figure 11 and **Videoclip S1**, the helix PNAGA-100@ Fe@ZIF-8 microrobots respond perfectly to the magnetic field to complete the task of walking a circle as designed. the PNAGA-100@ Fe@ZIF-8 microrobots were implemented with a rolling motion due to the friction from the substrate surface. The direction and speed of these microrobots can be modulated flexibly by the magnetic flux density and frequency according to different situations. Having thermal-triggered drug release capacity, good biocompatibility and good movability with the control of the magnetic field, our thermosensitive hydrogels-based magnetic microrobots have a great potential in drug delivery and cancer therapy.

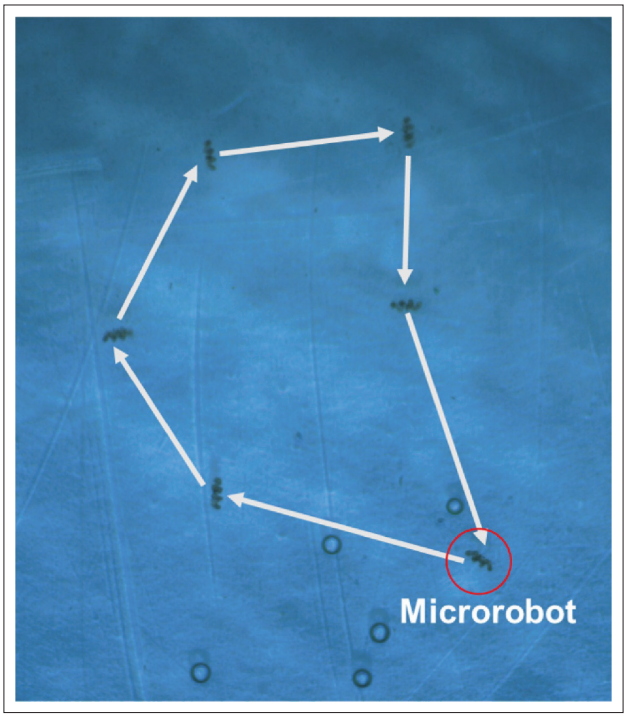

Figure 11. Motion control of helix PNAGA-100 thermosensitive microrobot under a magnetic actuator.

4. Conclusion

In conclusion, we developed a new method (3D printing) to prepare PNAGA-based hydrogels. Compared to the previously reported UV polymerization of PNAGA, PNAGA microrobots fabricated by 3D printing manifest more compact and accurate structures (from SEM). We have successfully endowed the PNAGA-based 3D-printed hydrogels with fast temperature-response ability. The thermosensitive properties of these microrobots are highly dependent on the NAGA monomer concentrations, from which PNAGA-100 exhibits the best thermosensitive performance with the maximum growth rate (22.5%) at 45°C. The mechanism of concentration determined thermosensitive performance has been proposed in relation to the polymerization density and intermolecular interactions. Drug release properties of PNAGA-100 microrobots were evaluated, and a two- to three times higher drug release amount was achieved at 45°C compared to 25°C, which are well in accordance with their thermosensitive properties. Furthermore, PNAGA-100-based thermosensitive microrobots were proven to be endowed with good biocompatibility and magnetic responsive ability, making them promising candidates for fulfilling various tasks *in vivo*. Fabricating PNAGA hydrogel-based microrobots by introducing advanced 3D printing technology is believed to be a genuine development engine for PNAGA hydrogels, benefiting their extensive applications in biomedical field in the future.

Acknowledgments

We gratefully acknowledge Ming Yang, a postgraduate student at the Southern University of Science and Technology, for helping with the SEM characterization.

Funding

This work is funded by the Shenzhen Institute of Artificial Intelligence and Robotics for Society (AC01202101106 [2020-ICP002]).

Conflict of interest

The authors declare no conflict of interest.

Author contributions

Conceptualization: Yan Zhou, Xiaopu Wang
Formal analysis: Yan Zhou, Min Ye
Investigation: Yan Zhou, Min Ye, Hongyu Zhao
Methodology: Yan Zhou
Writing – original draft: Yan Zhou
Writing – review & editing: Yan Zhou, Xiaopu Wang

Ethics approval and consent to participate

Not applicable.

Consent for publication

Not applicable.

Availability of data

Not applicable.

References

1. Aswathy SH, Narendrakumar U, Manjubala I, 2020, Commercial hydrogels for biomedical applications. *Heliyon*, 6(4):e03719.

   https://doi.org/10.1016/j.heliyon.2020.e03719

2. Gaharwar AK, Peppas NA, Khademhosseini A, 2014, Nanocomposite hydrogels for biomedical applications. *Biotechnol Bioeng*, 111(3):441–453.

   https://doi.org/10.1002/bit.25160

3. Kahn JS, Hu Y, Willner I, 2017, Stimuli-responsive DNA-based hydrogels: From basic principles to applications. *Acc Chem Res*, 50(4):680–690.

   https://doi.org/10.1021/acs.accounts.6b00542

4. Li Y, Yang HY, Lee DS, 2021, Advances in biodegradable and injectable hydrogels for biomedical applications. *J Control Release*, 330:151–160.

   https://doi.org/10.1016/j.jconrel.2020.12.008

5. Shi J, Yu L, Ding J, 2021, PEG-based thermosensitive and biodegradable hydrogels. *Acta Biomater,* 128:42–59.

   https://doi.org/10.1016/j.actbio.2021.04.009

6. Wahid F, Zhao X-J, Jia S-R, *et al.,* 2020, Nanocomposite hydrogels as multifunctional systems for biomedical applications: Current state and perspectives. *Compos B Eng*, 200:108208.

   https://doi.org/10.1016/j.compositesb.2020.108208

7. Chen L, Duan G, Zhang C, *et al.,* 2022, 3D printed hydrogel for soft thermo-responsive smart window. *Int J of Extrem Manuf*, 4(2):025302.

   https://doi.org/10.1088/2631-7990/ac5ae3

8. Boffito M, Sirianni P, Di Rienzo AM, *et al.,* 2015, Thermosensitive block copolymer hydrogels based on poly(varepsilon-caprolactone) and polyethylene glycol for biomedical applications: State of the art and future perspectives. *J Biomed Mater Res A,* 103(3):1276–1290.

   https://doi.org/10.1002/jbm.a.35253

9. Bozoglan BK, Duman O, Tunc S, 2020, Preparation and characterization of thermosensitive chitosan/carboxymethylcellulose/scleroglucan nanocomposite hydrogels. *Int J Biol Macromol,* 162:781–797.

   https://doi.org/10.1016/j.ijbiomac.2020.06.087

10. Fan R, Deng X, Zhou L, *et al.*, 2014, Injectable thermosensitive hydrogel composite with surface-functionalized calcium phosphate as raw materials. *Int J Nanomedicine*, 9:615–626.

    https://doi.org/10.2147/IJN.S52689

11. Zhan Z, Chen L, Duan H, *et al.,* 2021, 3D printed ultra-fast photothermal responsive shape memory hydrogel for microrobots. *Int J Extrem Manuf,* 4(1):015302.

    https://doi.org/10.1088/2631-7990/ac376b

12. Huang H, Qi X, Chen Y, *et al.,* 2019, Thermo-sensitive hydrogels for delivering biotherapeutic molecules: A review. *Saudi Pharm J*, 27(7):990–999.

    https://doi.org/10.1016/j.jsps.2019.08.001

13. Yuan M, Bi B, Huang J, *et al.,* 2018, Thermosensitive and photocrosslinkable hydroxypropyl chitin-based hydrogels for biomedical applications. *Carbohydr Polym*, 192:10–18.

    https://doi.org/10.1016/j.carbpol.2018.03.031

14. Zhang Y, Yu J, Ren K, *et al.,* 2019, Thermosensitive hydrogels as scaffolds for cartilage tissue engineering. *Biomacromolecules*, 20(4):1478–1492.

    https://doi.org/10.1021/acs.biomac.9b00043

15. He W, Ma Y, Gao X, *et al.,* 2020, Application of poly(N-isopropylacrylamide) as thermosensitive smart materials. *J Phys Conf Ser,* 1676(1):012063.

    https://doi.org/10.1088/1742-6596/1676/1/012063

16. Li J, Ma Q, Xu Y, *et al.,* 2020, Highly bidirectional bendable actuator engineered by LCST-UCST bilayer hydrogel with enhanced interface. *ACS Appl Mater Interfaces*, 12(49):55290–55298.

    https://doi.org/10.1021/acsami.0c17085

17. Li S, Wang W, Li W, *et al.,* 2021, Fabrication of thermoresponsive hydrogel scaffolds with engineered microscale vasculatures. *Adv Funct Mater*, 31(27):2102685.

    https://doi.org/10.1002/adfm.202102685

18. Tang L, Wang L, Yang X, *et al.,* 2021, Poly(N-isopropylacrylamide)-based smart hydrogels: Design, properties and applications. *Prog Mater Sci*, 115:100702.

    https://doi.org/10.1016/j.pmatsci.2020.100702

19. Xiao XC, 2007, Effect of the initiator on thermosensitive rate of poly(N-isopropylacrylamide) hydrogels. *Express Polym Lett*, 1(4):232–235.

    https://doi.org/10.3144/expresspolymlett.2007.35

20. Fu W, Zhao B, 2016, Thermoreversible physically crosslinked hydrogels from UCST-type thermosensitive ABA linear triblock copolymers. *Polym Chem*, 7(45):6980–6991.

    https://doi.org/10.1039/c6py01517d

21. Hua L, Xie M, Jian Y, *et al.,* 2019, Multiple-responsive and amphibious hydrogel actuator based on asymmetric UCST-type volume phase transition. *ACS Appl Mater Interfaces*, 11(46):43641–43648.

    https://doi.org/10.1021/acsami.9b17159

22. Xia M, Cheng Y, Meng Z, *et al.,* 2015, A novel nanocomposite hydrogel with precisely tunable UCST and LCST. *Macromol Rapid Commun*, 36(5):477–482.

    https://doi.org/10.1002/marc.201400665

23. Yu J, Wang K, Fan C, *et al.*, 2021, An ultrasoft self-fused supramolecular polymer hydrogel for completely preventing postoperative tissue adhesion. *Adv Mater*, 33(16):e2008395.

    https://doi.org/10.1002/adma.202008395

24. Xue X, Thiagarajan L, Braim S, *et al.,* 2017, Upper critical solution temperature thermo-responsive polymer brushes and a mechanism for controlled cell attachment. *J Mater Chem B*, 5(25):4926–4933.

    https://doi.org/10.1039/c7tb00052a

25. Ge S, Li J, Geng J, *et al.,* 2021, Adjustable dual temperature-sensitive hydrogel based on a self-assembly cross-linking strategy with highly stretchable and healable properties. *Mater Horiz*, 8(4):1189–1198.

    https://doi.org/10.1039/d0mh01762k

26. Wu Y, Wang H, Gao F, *et al.*, 2018, An injectable supramolecular polymer nanocomposite hydrogel for prevention of breast cancer recurrence with theranostic and mammoplastic functions. *Adv Funct Mater*, 28(21):1801000.

    https://doi.org/10.1002/adfm.201801000

27. Xu Z, Liu W, 2018, Poly(N-acryloyl glycinamide): A fascinating polymer that exhibits a range of properties from UCST to high-strength hydrogels. *Chem Commun(Camb)*, 54(75):10540–10553.

    https://doi.org/10.1039/c8cc04614j

28. Boustta M, Vert M, 2020, Hyaluronic acid-poly(N-acryloyl glycinamide) copolymers as sources of degradable thermoresponsive hydrogels for therapy. *Gels*, 6(4):E42.

    https://doi.org/10.3390/gels6040042

29. Yang D, Eronen H, Tenhu H, *et al.*, 2021, Phase transition behavior and catalytic activity of poly(N-acryloylglycinamide-co-methacrylic acid) microgels. *Langmuir*, 37(8):2639–2648.

    https://doi.org/10.1021/acs.langmuir.0c03264

30. Bunea A-I, del Castillo Iniesta N, Droumpali A, *et al.*, 2021, Micro 3D printing by two-photon polymerization: Configurations and parameters for the nanoscribe system. *Micro*, 1:164–180.

    https://doi.org/10.3390/micro1020013

31. Faraji Rad Z, Prewett PD, Davies GJ, 2021, High-resolution two-photon polymerization: The most versatile technique for the fabrication of microneedle arrays. *Microsyst Nanoeng*, 7:71.

    https://doi.org/10.1038/s41378-021-00298-3

32. Koskela JE, Turunen S, Ylä-Outinen L, *et al.*, 2012, Two-photon microfabrication of poly(ethylene glycol) diacrylate and a novel biodegradable photopolymer-comparison of processability for biomedical applications. *Polym Adv Technol*, 23(6):992–1001.

    https://doi.org/10.1002/pat.2002

33. Petcu EB, Midha R, McColl E, *et al.*, 2018, 3D printing strategies for peripheral nerve regeneration. *Biofabrication*, 10(3):032001.

    https://doi.org/10.1088/1758-5090/aaaf50

34. Tao J, He Y, Wang S, *et al.*, 2019, 3D-printed nerve conduit with vascular networks to promote peripheral nerve regeneration. *Med Hypotheses*, 133:109395.

    https://doi.org/10.1016/j.mehy.2019.109395

35. Weisgrab G, Guillaume O, Guo Z, *et al.*, 2020, 3D printing of large-scale and highly porous biodegradable tissue engineering scaffolds from poly(trimethylene-carbonate) using two-photon-polymerization. *Biofabrication*, 12(4):045036.

    https://doi.org/10.1088/1758-5090/abb539

36. Lee SJ, Esworthy T, Stake S, *et al.*, 2018, Advances in 3D bioprinting for neural tissue engineering. *Adv Biosyst*, 2:1700213.

    https://doi.org/10.1002/adbi.201700213

37. Lee JW, 2015, 3D nanoprinting technologies for tissue engineering applications. *J Nanomater*, 2015:1–14.

    https://doi.org/10.1155/2015/213521

38. Terzopoulou A, Wang X, Chen XZ, *et al.*, 2020, Biodegradable metal-organic framework-based microrobots (MOFBOTs). *Adv Healthc Mater*, 9:e2001031.

    https://doi.org/10.1002/adhm.202001031

39. Wang X, Qin X-H, Hu C, *et al.*, 2018, 3D printed enzymatically biodegradable soft helical microswimmers. *Adv Funct Mater*, 28:1804107.

    https://doi.org/10.1002/adfm.201804107

40. Jiang Z, Tan ML, Taheri M, *et al.*, 2020, Strong, self-healable, and recyclable visible-light-responsive hydrogel actuators. *Angew Chem Int Ed Engl*, 59(18):7049–7056.

    https://doi.org/10.1002/anie.201916058

41. Song X, Zhang Z, Zhu J, *et al.*, 2020, Thermoresponsive hydrogel induced by dual supramolecular assemblies and its controlled release property for enhanced anticancer drug delivery. *Biomacromolecules*, 21(4):1516–1527.

    https://doi.org/10.1021/acs.biomac.0c00077

42. Peng X, Liu T, Jiao C, *et al.*, 2017, Complex shape deformations of homogeneous poly(N-isopropylacrylamide)/graphene oxide hydrogels programmed by local NIR irradiation. *J Mater Chem B*, 5(39):7997–8003.

    https://doi.org/10.1039/c7tb02119d

43. Bian Q, Fu L, Li H, 2022, Engineering shape memory and morphing protein hydrogels based on protein unfolding and folding. *Nat Commun*, 13(1):137.

    https://doi.org/10.1038/s41467-021-27744-0

44. Xu Z, Fan C, Zhang Q, *et al.*, 2021, A self-thickening and self-strengthening strategy for 3D printing high-strength and antiswelling supramolecular polymer hydrogels as meniscus substitutes. *Adv Funct Mater*, 31(18):2100462.

    https://doi.org/10.1002/adfm.202100462

45. Wang X, Chen XZ, Alcantara CCJ, *et al.*, 2019, MOFBOTS: Metal-organic-framework-based biomedical microrobots. *Adv Mater*, 31:e1901592.

    https://doi.org/10.1002/adma.201901592